JACS
JOURNAL OF THE AMERICAN CHEMICAL SOCIETY

Article

pubs.acs.org/JACS

Molecular Catalysis of H_2 Evolution: Diagnosing Heterolytic versus Homolytic Pathways

Cyrille Costentin,* Hachem Dridi, and Jean-Michel Savéant*

Université Paris Diderot, Sorbonne Paris Cité, Laboratoire d'Electrochimie Moléculaire, UMR 7591 CNRS, 15 rue Jean-Antoine de Baïf, F-75205 Paris Cedex 13, France

Supporting Information

ABSTRACT: Molecular catalysis of H_2 production from the electrochemical reduction of acids by transition-metal complexes is one of the key issues of modern energy challenges. The question of whether it proceeds heterolytically (through reaction of an initially formed metal hydride with the acid) or homolytically (through symmetrical coupling of two molecules of hydride) has to date received inconclusive answers for a quite simple reason: the theoretical bases for criteria allowing the distinction between homolytic and heterolytic pathways in nondestructive methods such as cyclic voltammetry have been lacking heretofore. They are provided here, allowing the distinction between the two pathways. The theoretical predictions and the diagnosing strategy are illustrated by catalysis of the reduction of phenol, acetic acid, and protonated triethylamine by electrogenerated iron(0) tetraphenylporphyrin. Rather than being an intrinsic property of the catalytic system, the occurrence of either a heterolytic or a homolytic pathway results from their competition as a function of the concentrations of acid and catalyst and the rate constants for hydride formation and H_2 evolution by hydride protonation or dimerization.

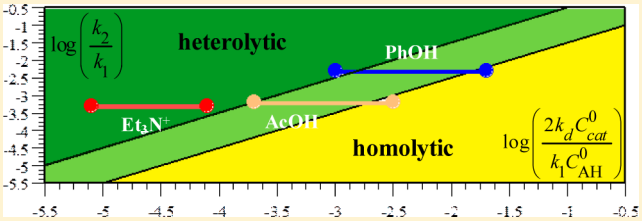

INTRODUCTION

In addition to its fundamental interest, the ongoing attention attracted by catalysis of the production of hydrogen upon reduction of acids has a double motivation. One aims at a better understanding of hydrogenases.[1−6] The other is of a synthetic nature and relates to modern energy challenges.[7−12] Whether the reaction follows a homolytic or heterolytic reaction pathway, as illustrated by Scheme 1,[13,14] is a question that has been addressed for a long time[15] and continues to be a debated issue.[16−20] Diverging conclusions have often been reached even with the same catalyst or closely related catalysts. This is the case with the popular cobaloxime H_2 evolution catalysts. They were first considered to follow a homolytic pathway,[8b,16a,19] whereas more recent studies favor a heterolytic pathway.[20] Several quantum-chemical calculations of thermodynamic quantities that may help suggest which is the preferred reaction pathway have been carried out, also favoring the heterolytic pathway.[17,18,20c]

Cyclic voltammetry (CV) has been widely used to investigate the reaction mechanism. However, reliable mechanistic conclusions could not be reached for the simple reason that theoretical relationships and the ensuing diagnostic criteria are lacking for reaction schemes corresponding to homolytic pathways and to their competition with heterolytic pathways. One may resort to "digital simulation"[21] of experimental cyclic voltammograms. However, the number of parameters is so large that many different schemes with ad hoc parameter values can match the data, thus preventing any effective determination of the reaction mechanism. Digital simulations may be quite useful to finalize the mechanism determination, but they should be prepared by an analysis of the diffusion−reaction problem leading to the identification of the minimal number of governing dimensionless parameters.

The aim of the present contribution is to provide these lacking relationships and the ensuing diagnostic criteria. On the basis of these criteria, strategies allowing the distinction between the two types of reaction pathways and the identification of the parameters that govern their competition will be proposed. These strategies will be illustrated by an experimental example, namely, catalysis of the reduction of phenol, acetic acid, and protonated triethylamine in *N*,*N*′ dimethylformamide (DMF) by electrogenerated iron(0) tetraphenylporphyrin (Fe^0TPP).

RESULTS AND DISCUSSION

1. Reminder of the Characteristics of a Simple One-Electron−One-Step Catalytic Reaction Scheme. For a simple catalytic reaction scheme, the catalytic CV response may exhibit diverse shapes that are summarized in Figure 1. Since we are interested in efficient catalysts, the global catalytic rate constant is implied to be large, and therefore, "pure kinetic conditions" are achieved, corresponding to the upper three zones in Figure 1. Under the assumption that enough acid is present to render its consumption negligible in the course of the CV run, the kinetic situation belongs to the upper right-hand zone in Figure 1. An S-shaped CV response is thus

Received: June 10, 2014
Published: September 4, 2014

   dx.doi.org/10.1021/ja505845t | J. Am. Chem. Soc. 2014, 136, 13727−13734

Scheme 1. EEPDimP Pathways[a,b]

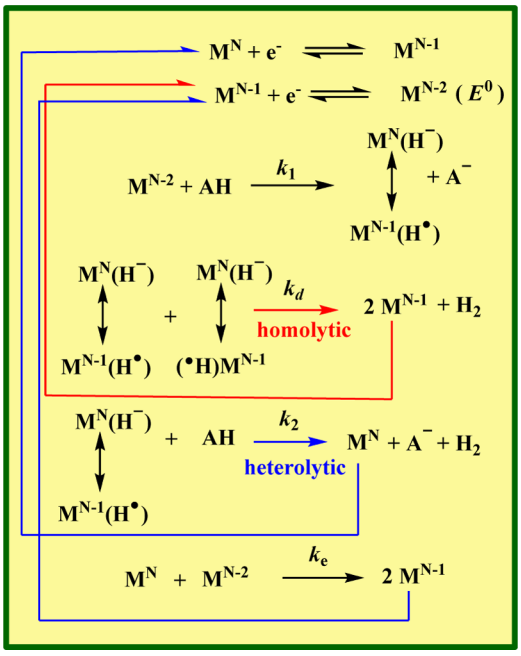

[a]M^J ($J = N, N-1, N-2$) denotes a complex with a metal at the oxidation degree J. The vertical double-headed arrow indicates resonance between two forms of the metal complex. AH denotes the acid and A^- its conjugated base. The k's are the corresponding rate constants. [b]The acronym EEPDimP describes the nature and sequencing of the successive steps. E denotes electrode electron transfer, P denotes protonation, and Dim denotes the H_2-evolving dimerization step. This scheme was adapted from a more general formalism[22a] to make it more specific to the present case.

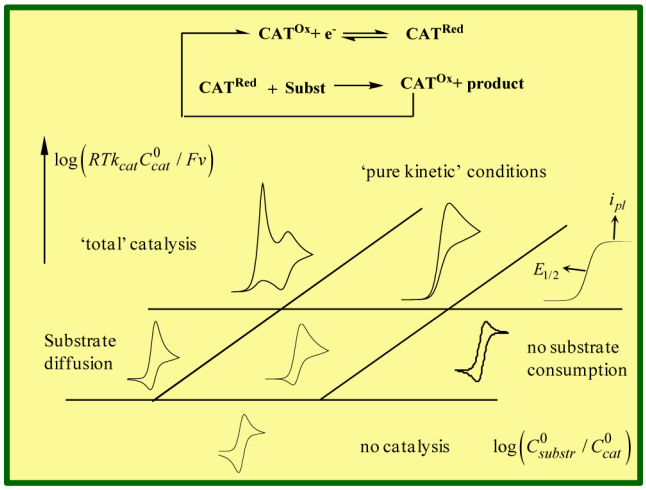

Figure 1. Zone diagram showing the different shapes of the CV response as a function of the dimensionless rate (ordinate) and excess (abscissa) parameters.[22b,c]

expected, being characterized by a plateau current i_{pl} and a half-wave potential $E_{1/2}$.

2. Competition between the Heterolytic and Homolytic Pathways in the Framework of Scheme 1. The same assumptions as in the preceding section are made in the following discussion of the heterolytic versus homolytic competition of Scheme 1. Within this framework, the S-shaped CV responses depend upon three dimensionless parameters [see the Supporting Information (SI)]:

$$\frac{k_2}{k_1}, \quad \frac{k_d C^0_{cat}}{k_1 C^0_{AH}}, \quad \text{and} \quad \frac{k_e C^0_{cat}}{k_1 C^0_{AH}}$$

where C^0_{cat} and C^0_{AH} are the concentrations of catalyst and acid, respectively, and the rate constants k are defined in Scheme 1. The first two parameters measure the rapidity of the second protonation step and the dimerization step, respectively, relative to the first protonation step. They are indicative of the propensity of the key intermediate $M^N(H^-) \leftrightarrow M^{N-1}(H^•)$ to be or not be at steady state. In each of these cases, the ratio of the two first parameters provides a measure of the competition between the second protonation step and dimerization, i.e., the competition between the heterolytic and homolytic pathways. The third parameter is related to the reduction of the M^N complex, which closes the catalytic loop. It may take place at the electrode surface or in the solution by reaction with the M^{N-2} complex. If k_1 is large, the M^N complex (like other intermediates) is formed close to the electrode surface and is reduced before it has time to meet and react with the M^{N-2} complex (ECE-type situation), and vice versa for large values of $k_e C^0_{cat}/k_1 C^0_{AH}$ [the solution electron transfer (SET) situation].

We first examine the SET situation ($k_e C^0_{cat}/k_1 C^0_{AH} \rightarrow \infty$). The zone diagram in Figure 2 summarizes the characteristics of the S-shaped CV response as a function of the two parameters k_2/k_1 and $k_d C^0_{cat}/k_1 C^0_{AH}$. The kinetic zones are obtained upon giving extreme values to these parameters (0 and ∞, respectively) so as to reach simplified behaviors that depend on a lesser number of parameters (one and zero, respectively). Because of experimental uncertainties in measuring plateau currents (~5%) and half-wave potentials (~5 mV), these simpler behaviors are reached for finite small and large values of the dimensionless parameters, respectively. In the determination of the boundaries between zones, the simplest zone is privileged (zero-parameter zone over one-parameter zone, one-parameter zone over two-parameter zone, and so forth). The area of the two-parameter zone G (where G = "general") is thus minimized at the benefit of the one- and zero-parameter zones. The meaning of the various zones and the corresponding expressions for the plateau currents and half-wave potentials are detailed in the caption of Figure 2. Derivations of these expressions are provided in the SI.

The ECE situation ($k_e C^0_{cat}/k_1 C^0_{AH} \rightarrow 0$), gives rise to another zone diagram (Figure 3). It is not very different from the SET zone diagram (Figure 2), and the expressions for the plateau currents and half-wave potentials are similar albeit not identical in the two cases.

Mechanism diagnosis derives from the combined observation of the plateau current and half-wave potential and their variation or lack of variation with the acid and catalyst concentrations according to the equations in the ellipsoidal inserts that characterize the zero-parameter zones. The working curves in the rectangular insets indicate the variations to be expected when passing from one zero-parameter zone to the other upon variation of the catalyst and acid concentrations. An estimate of the three rate constants ensues. The reliability of the diagnostic is then checked by means of digital simulation, and the values of the rate constants are simultaneously adjusted for an improved fit of the experimental data.

dx.doi.org/10.1021/ja505845t | J. Am. Chem. Soc. 2014, 136, 13727−13734

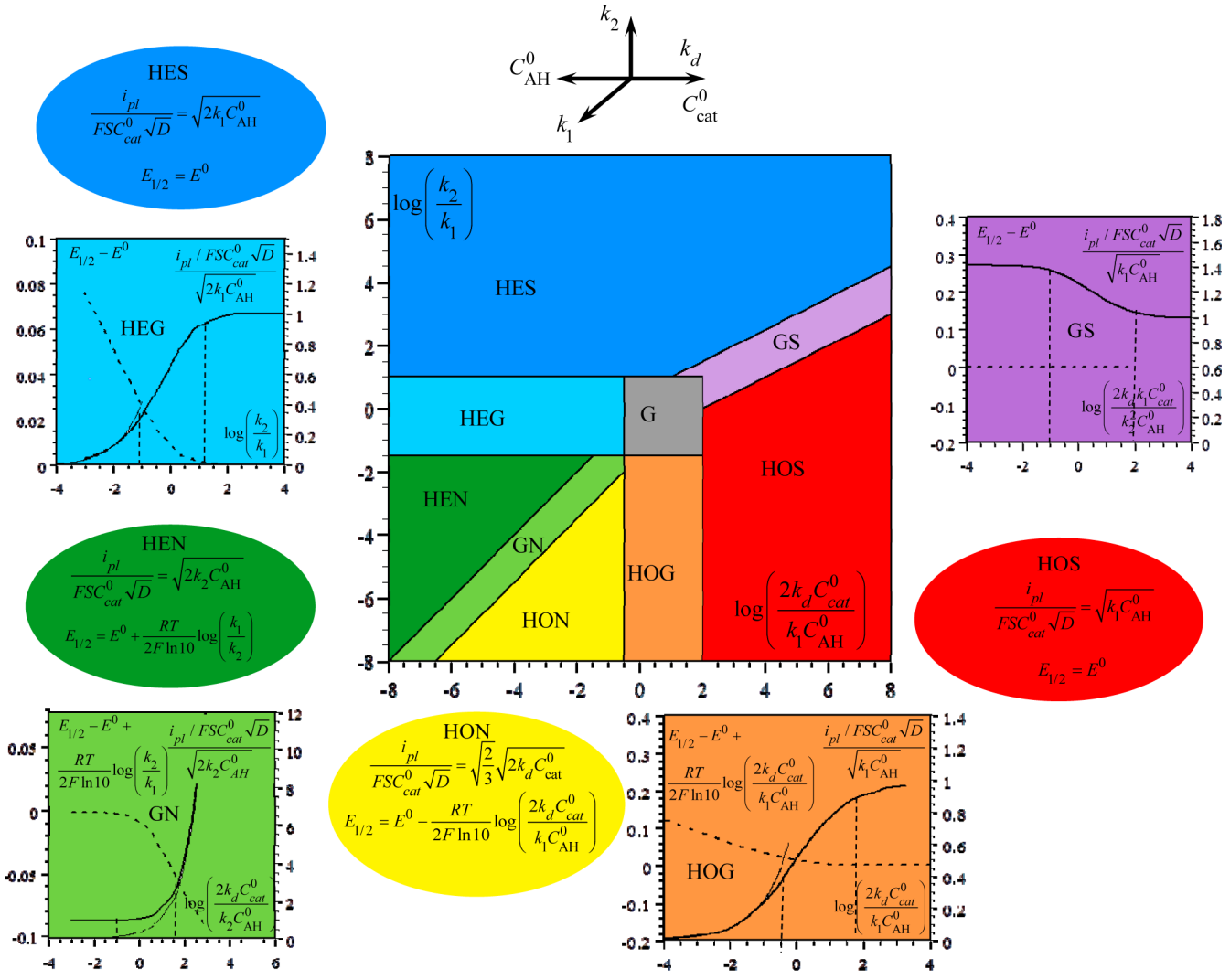

Figure 2. Competition between the heterolytic and homolytic pathways in the SET regime ($k_e C^0_{cat}/k_1 C^0_{AH} \rightarrow \infty$). The zone diagram summarizes the various kinetic behaviors as a function of the two dimensionless parameters k_2/k_1 and $k_d C^0_{cat}/k_1 C^0_{AH}$. The zones are labeled using the following abbreviations: HE, heterolytic; HO, homolytic; S, steady-state; N, non-steady-state; G, general. The effects of the experimental parameters contained in the dimensionless parameters are summarized, as logarithms, by the set of arrows on top of the diagram, which allows traveling through the various zones. The blue (HES) and green (HEN) zones correspond to heterolytic pathways in which the key intermediate $M^N(H^-) \leftrightarrow M^{N-1}(H^\bullet)$ is or is not in steady state, respectively. Likewise, the red (HOS) and yellow (HON) zones corresponds to homolytic pathways in which the key intermediate $M^N(H^-) \leftrightarrow M^{N-1}(H^\bullet)$ is or is not in steady state, respectively. In these four cases, closed-form expressions for the current and half-wave potential apply. They are given in the oval inset of the same color as the corresponding zone. Within the heterolytic case, the passage from the steady-state regime to the non-steady-state regime occurs through zone HEG. The variations of the plateau current (thick black line) and half-wave potential (dotted line) with the appropriate parameter are shown as working curves in the square inset of the same color (cyan). The thin line corresponds to the variation of the plateau current in the corresponding limiting zone. Vertical dashed lines indicate the boundaries between the zones. The same applies, within the homolytic case, to the passage from the steady-state regime to the non-steady-state regime through zone HOG (orange). The magenta zone (GS) depicts the passage from the heterolytic pathway to the homolytic pathway in the steady-state regime. Here the variations of the current and half-wave potential are given against a dimensionless parameter that directly represents the competition between the two pathways. The same applies to the light-green zone (GN), which depicts the passage from the heterolytic pathway to the homolytic pathway in the non-steady-state regime, although a different dimensionless competition parameter is used. The boundaries between the zones correspond to a 10% uncertainty of the plateau current and a 5 mV uncertainty in the half-wave potential. The potentials are given in volts. *S* is the electrode surface area, and *D* is the catalyst diffusion coefficient.

The easiest situation is when the expressions for the plateau current and half-wave potential are different when passing from one zero-parameter zone to the other, allowing the distinction between the two zones by means of the variation or lack of variation of the plateau current and half-wave potential as the acid and catalyst concentrations are varied. In the converse case, where these formal expressions for the plateau current and half-wave potential are the same, as for example in the case of zones HES and HOS, one may have the impression that making a distinction between the two zones is impossible. In fact, the following strategy may be applied. The expressions for the plateau current differ by a factor of 2 or $\sqrt{2}$ upon crossing the transition zone GS. Consequently, if the transition zone is reached upon changing the acid and/or catalyst concentration, the distinction between the HES and HOS zones becomes possible. If no transition zone is observed, then a guess can be made that the system is in either the HES zone or the HOS zone, and k_1 may be estimated in each case. In addition, the

dx.doi.org/10.1021/ja505845t | J. Am. Chem. Soc. 2014, 136, 13727−13734

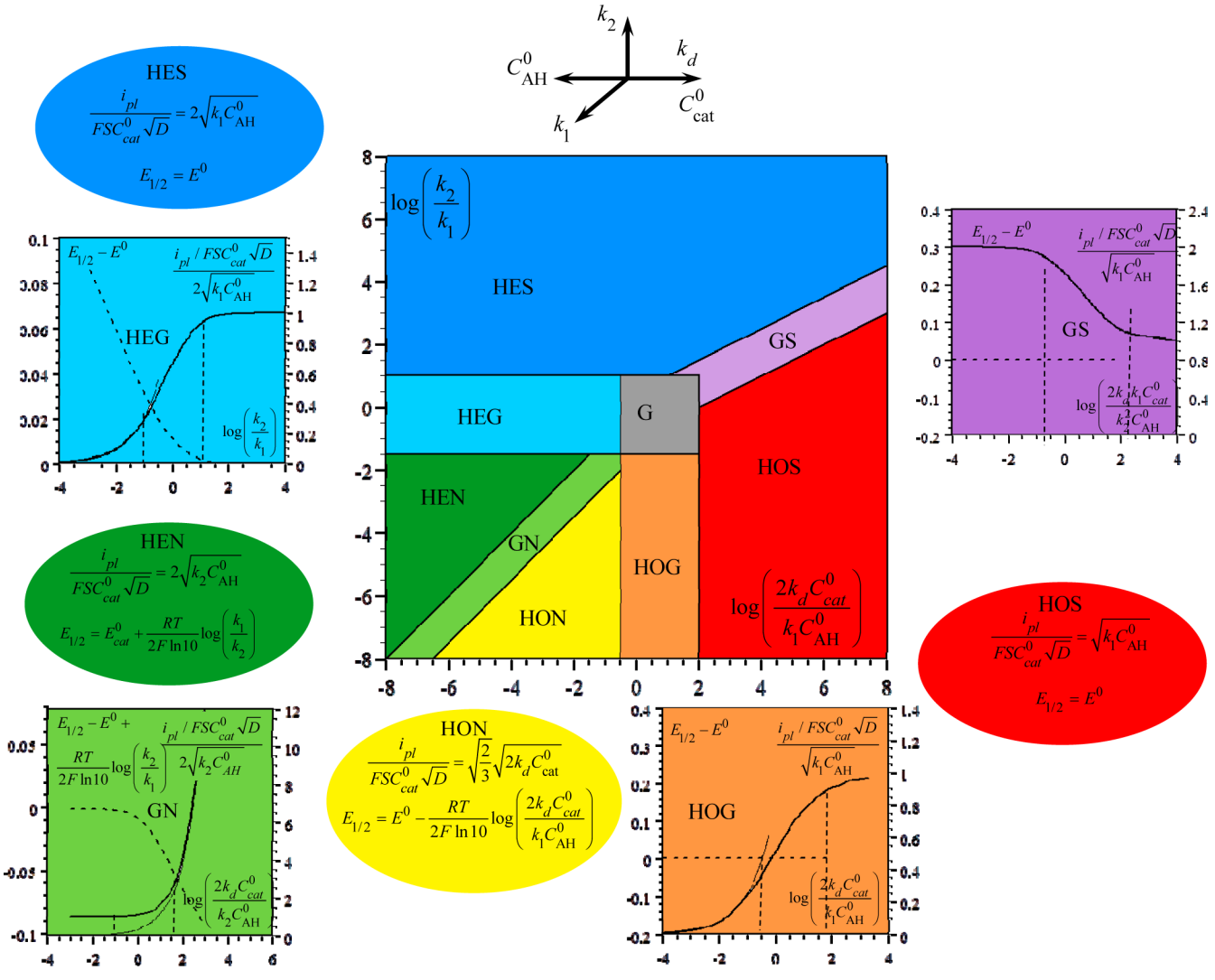

Figure 3. Competition between the heterolytic and the homolytic pathways in the ECE regime ($k_eC^0_{cat}/k_1C^0_{AH} \rightarrow 0$). This zone diagram uses the same definitions and characteristics as in Figure 2. The plateau currents in the HES and HEN zones (and in the corresponding transition zones) are modified in comparison with the SET regime.

absence of a transition zone implies that $2k_dC^0_{cat}/k_1C^0_{AH}$ is either <100 (HES) or >100 (HOS). The ensuing values of k_d, being smaller or not smaller than the diffusion limit, finally allow the effective distinction between the two zones.

The next section is dedicated to an experimental illustration of these procedures.

3. Catalysis of the Reduction of Protonated Triethylamine, Phenol, and Acetic Acid in DMF by Electrogenerated Fe^0TPP: Raw CV Data. Figure 4 summarizes the CV data obtained with the three acids, using the concentrations of acid and catalyst as operational parameters to move the point representing the system in the zone diagram (Figures 2 and 3). In the absence of acid (Figure 4, top left), the CV response exhibits two reversible waves corresponding to the first two electron transfer steps in Scheme 1, with standard potentials (E^0) equal to −1.34 and −2.04 V vs Fc^+/Fc, respectively. One consequence of this potential sequencing is that the SET reaction at the end of Scheme 1 is strongly downhill and consequently endowed with a rate constant k_e that is most likely close to the diffusion limit in all three cases. We know from previous work[23] that the iron(II) hydride formed upon electron transfer to the iron(0) complex is more difficult to reduce than the iron(I) complex. This observation validates the reaction sequence represented in Scheme 1 rather than other sequences of electron transfers, proton transfers, and dimerization steps, which are briefly discussed in section 6. Of the three acids, Et_3NH^+ is the most acidic (pK = 9.2 in DMF[24]). The first protonation step is thus expected to be the most rapid in the series. This is the reason that we used scan rates of 10, 15, and 20 V s^{-1} (Figure 4, top right, where only the 10 V s^{-1} data are shown), which are relatively high in order to minimize side phenomena starting from acid consumption[25] but still low enough for pure kinetic conditions to remain fulfilled (see Figure 1). With the weaker acids AcOH and PhOH (pK = 13.2 and 18.8, respectively[24]), catalysis is less vigorous (Figure 4, middle and bottom), and a scan rate of 2 V s^{-1} offers a good compromise for minimizing the side effects while preserving the pure kinetic conditions.

4. Catalysis of the Reduction of Protonated Triethylamine, Phenol, and Acetic Acid in DMF by Electrogenerated Fe^0TPP: Treatment of the CV Data. Because Et_3NH^+ is the strongest acid of the series and gives rise to

dx.doi.org/10.1021/ja505845t | J. Am. Chem. Soc. 2014, 136, 13727−13734

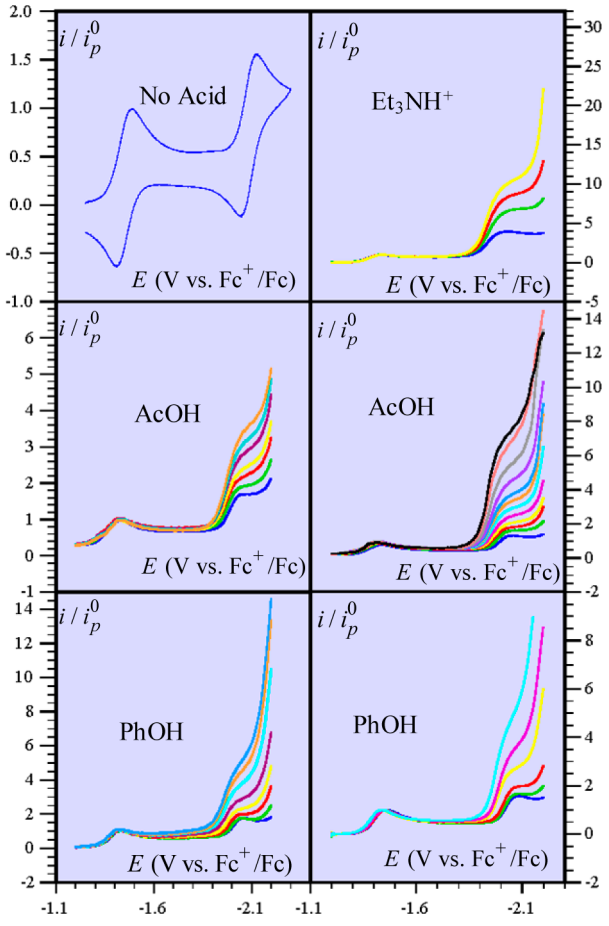

Figure 4. Cyclic voltammetry of $Fe^{II}TPP$ in DMF + 0.1 M *n*-Bu_4NPF_6. Top left: 1 mM $Fe^{II}TPP$ in the absence of acid at 0.1 V s^{-1}. Top right: 1 mM $Fe^{II}TPP$ at 10 V s^{-1} in the presence of Et_3NH^+(M): 0.0061 (blue), 0.0134 (green), 0.0219 (red), 0.0301 (yellow), 0.0421 (magenta), 0.0664 (cyan). Middle left: 1 mM $Fe^{II}TPP$ at 2 V s^{-1} in the presence of AcOH (M): 0.029 (blue), 0.054 (green), 0.084 (red), 0.124 (yellow), 0.174 (magenta), 0.224 (cyan), 0.274 (orange). Middle right: 5 mM $Fe^{II}TPP$ at 2 V s^{-1} in the presence of AcOH (M): 0.01 (blue), 0.03 (green), 0.055 (red), 0.085 (yellow), 0.125 (magenta), 0.175 (cyan), 0.225 (orange), 0.275 (light blue), 0.375 (purple), 0.5 (gray), 0.7 (light red), 0.9 (black). Bottom left: 1 mM $Fe^{II}TPP$ at 2 V s^{-1} in the presence of PhOH (M): 0.18 (blue), 0.355 (green), 0.68 (red), 1 (yellow), 1.24 (magenta), 1.72 (cyan), 2 (orange), 2.3 (light blue). Bottom right: 5 mM $Fe^{II}TPP$ at 2 V s^{-1} in the presence of PhOH (M): 0.18 (blue), 0.355 (green), 0.68 (red), 1.24 (yellow), 1.72 (magenta), 2.3 (cyan). i_p^0 is the peak current of the one-electron Nernstian $Fe^{I/0}$ wave at the same scan rate in the absence of acid [$i_p^0 = 0.446FSC_{cat}^0D^{1/2}(Fv/RT)^{1/2}$].

efficient catalysis, we may infer that k_1 is large and therefore that the kinetic regime is likely to be of the ECE type. We may thus analyze the data in this framework, i.e., using the zone diagram of Figure 3 and the accompanying expressions and working curves. The experimental values of the normalized plateau current i_{pl}/i_p^0 (where i_p^0 is the peak current of the one-electron Nernstian $Fe^{I/0}$ wave at the same scan rate in the absence of acid) and the half-wave potential $E_{1/2}$ (referred to the catalyst standard potential E^0) are plotted against the square root of the acid concentration in Figure 5. The proportionality of the plateau current to the square root of the acid concentration and the constancy of the half-wave potential at a positive value relative to the standard potential of the catalyst are two diagnostic criteria that point to the system being

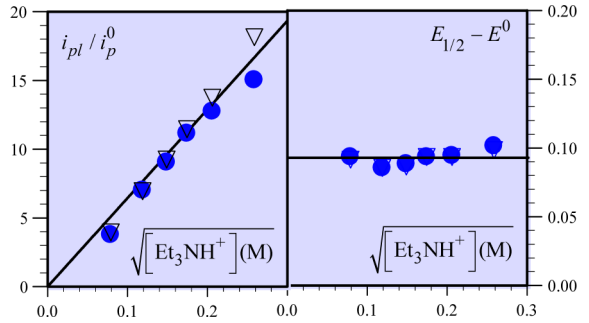

Figure 5. Catalysis of the reduction of Et_3NH^+ by electrogenerated Fe^0TPP. Shown are plots of the normalized plateau current (left) and the half-wave potential referred to the catalyst standard potential (right) against the square root of the acid concentration. [FeTPP] = 1 mM. Blue dots: experimental data from the top-right panel of Figure 4. Open triangles: simulation.

unambiguously in the HEN zone, i.e., following a heterolytic pathway with the hydride key intermediate not being at steady state. Applying the relationships given in Figure 3 for the HEN zone leads to the values of k_1 and k_2 listed in Table 1.[26] Taking

Table 1. Rate Constants (M^{-1} s^{-1})

acid	k_1	k_2	k_d
Et_3NH^+	2×10^8	10^5	–
AcOH	10^6	6.5×10^2	3×10^4
PhOH	5×10^3	25	10^4

k_e as equal to 2×10^8 M^{-1} s^{-1} leads to values of the parameter $k_eC_{cat}^0/k_1C_{AH}^0$ smaller than 1 over the whole range, thus justifying the assumption of an ECE regime. Simulation[27] of the variations of the plateau current and of the half-wave potential using the values of the rate constants thus estimated confirms these conclusions (Figure 5).

We come now to PhOH, which gives rise to the smallest catalytic currents in the series and is therefore likely to fall within the SET regime. The data (Figure 4 bottom) were treated accordingly, giving rise to the variations of the plateau current and the half-wave potential versus the square root of the acid concentration shown in Figure 6. There is a clear deviation of the plateau current from proportionality to the square root of the acid concentration upon decreasing the acid

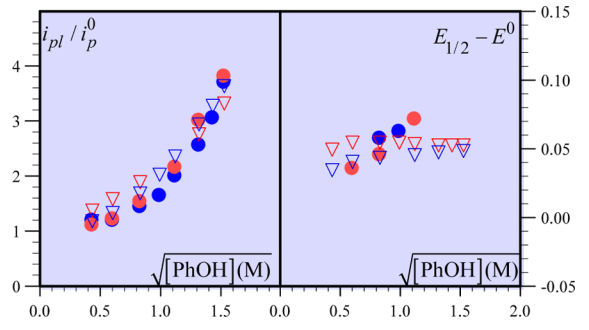

Figure 6. Catalysis of the reduction of PhOH by electrogenerated Fe^0TPP. Shown are plots of the normalized plateau current (left) and the half-wave potential referred to the catalyst standard potential (right) against the square root of the acid concentration. [FeTPP] = 1 mM (blue symbols) or 5 mM (red symbols). Dots: experimental data from the bottom panels of Figure 4. Open triangles: simulation.

dx.doi.org/10.1021/ja505845t | J. Am. Chem. Soc. 2014, 136, 13727−13734

concentration and increasing the catalyst concentration, indicating that the system is traveling across zone GN in the zone diagram in Figure 2 (also see the expanded view of zones HEN, GN, and HON in Figure 8). Determination of the rate constants was done as follows. The data obtained at high PhOH concentrations are assumed to correspond to the HEN zone. The plateau current and half-wave potential obtained under these conditions thus allowed the determination of k_1 and k_2 (Table 1). On the basis of these values, simulation[27] of the voltammograms over the whole PhOH concentration range led to the value of k_d (Table 1). This procedure allows taking into account deviations of the cyclic voltammograms from pure kinetic conditions (see Figure 1), which are assumed in the zone diagram but are no longer fulfilled when the phenol concentration is decreased because of the small catalytic rate constants. We may note that the variation of the half-wave potential with the concentrations is of no practical use because of the large uncertainties deriving from the proximity of a second catalytic wave that became very high as the acid concentration was raised and thus artificially pushed the first catalytic wave toward more positive values (Figure 4 bottom). Taking again a value of 2×10^8 M^{-1} s^{-1} for k_e leads to values of the parameter $k_eC^0_{cat}/k_1C^0_{AH}$ that are larger than 10 over the whole range of the two concentrations, thus justifying the assumption of an SET regime.

The variations of the plateau current and the half-wave potential versus the square root of the acid concentration observed with AcOH are shown in Figure 7 for two values of the catalyst concentration (1 and 5 mM). The data were analyzed in the framework of the SET regime, as suggested by the fact that the catalysis is not very vigorous as it is with

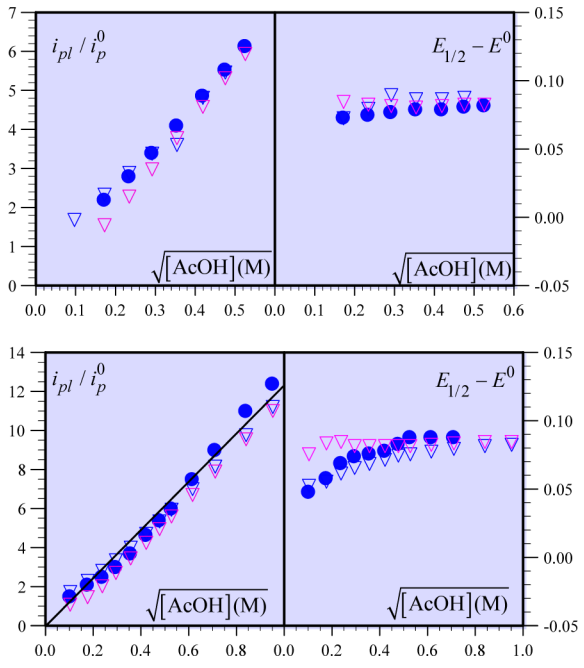

Figure 7. Catalysis of the reduction of AcOH by electrogenerated Fe^0TPP. Shown are plots of the normalized plateau current (left) and the half-wave potential referred to the catalyst standard potential (right) against the square root of the acid concentration. Top: [FeTPP] = 1 mM. Bottom: [FeTPP] = 5 mM. Blue dots: experimental data from the middle panels of Figure 4. Open triangles: simulations for heterolytic + homolytic pathways (blue) and the heterolytic pathway alone (magenta).

PhOH. We note a slight deviation of the plateau current plot from proportionality to the square root of the acid concentration at low acid concentrations. This observation points to the interference of a homolytic pathway in this concentration range. The values of k_1 and k_2 may be determined from the large linear portion of the i/i_p^0 plot at high acid concentrations and from the value of $E_{1/2}$ in the same concentration range, leading to $k_1 = 10^6$ M^{-1} s^{-1} and $k_2 = 10^3$ M^{-1} s^{-1}. The SET versus ECE parameter varies as $0.2 \leq k_eC^0_{cat}/k_1C^0_{AH} \leq 30$ within the range of acid and catalyst concentrations. It follows that the system is not exactly under the SET regime, calling for a slight correction of k_1 and k_2 obtained by means of simulation and finally leading to the values reported in Table 1. The variations of the half-wave potential at 1 mM catalyst concentration (Figure 7, top right) are not precise enough to corroborate the interference of a homolytic pathway as noted earlier. However, this is clearly confirmed by the $E_{1/2}$ data obtained at a catalyst concentration of 5 mM (Figure 7, bottom right). Simulations[27] allowed adjustment of the k_d value to reproduce the experimental data.

5. Comparison of the Three Acids. On the basis of the data summarized in Table 1, an expanded view of the bottom-left corner of the zone diagram (Figure 8) shows that the key

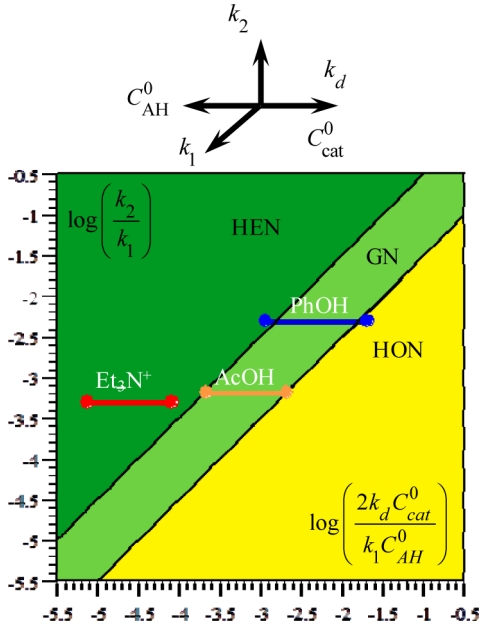

Figure 8. Expanded view of the zone diagram showing how the system travels through the heterolytic-to-homolytic transition zone as a function of the nature of the acid, its concentration, and the concentration of catalyst.

intermediate $M^N(H^-) \leftrightarrow M^{N-1}(H^\bullet)$ is not at steady state for all three systems. The reduction of the strongest acid, Et_3NH^+, follows an entirely heterolytic reaction pathway, whereas the two other concurrently take a heterolytic and a homolytic path. It also interesting to note that the two protonation rate constants are linearly correlated with the pK of the acid (Figure 9).

6. Alternative Reaction Pathways. Besides the EEPDimP pathways (Scheme 1) that we have investigated so far, one may alternatively consider two other sequences of the E, P, dim, and P steps within the reaction pathway, as shown in Schemes 2 and 3. The variations of the plateau current and half-wave

dx.doi.org/10.1021/ja505845t | J. Am. Chem. Soc. 2014, 136, 13727−13734

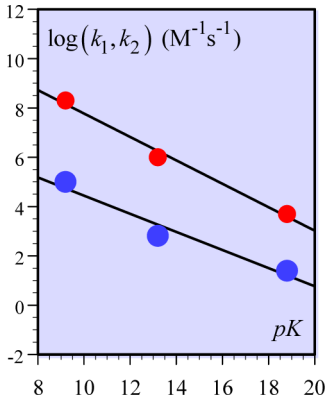

Figure 9. Correlations of the two protonation rate constants k_1 (red dots) and k_2 (blue dots) with the pK of the acid.

Scheme 2. EPEDimP Pathways

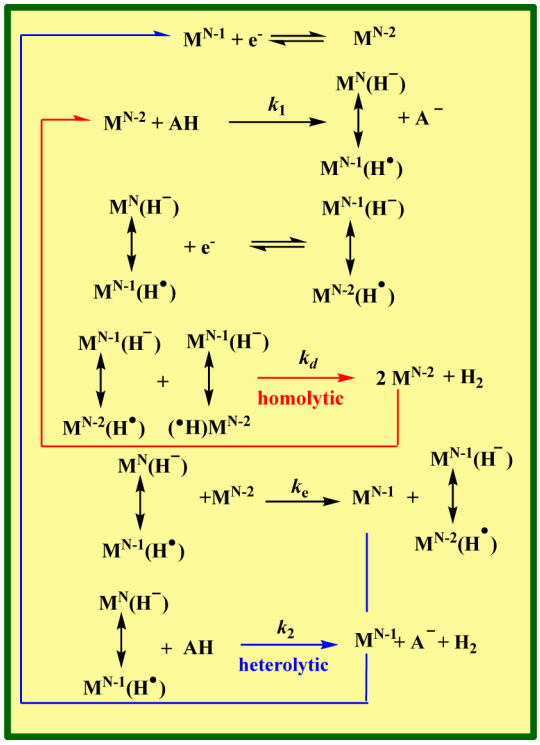

potential for these pathways should then be analyzed in a quite similar manner by means of zone diagrams accompanied by adapted expressions and working curves that can be used to unravel the heterolytic/homolytic competition.

CONCLUDING REMARKS

(1) The outcome of this work is that we now have theoretical tools that allow diagnosis of the occurrence of heterolytic versus homolytic pathways in the catalysis of H_2 evolution from reduction of acids.

(2) Rather than being an intrinsic property of the catalytic system, the occurrence of either a heterolytic or a homolytic pathway results from their competition as a function of the concentrations of acid and catalyst and of the rate constants for hydride formation and H_2 evolution by hydride protonation or dimerization. The use of a kinetic zone diagram based on a minimal number of dimensionless parameters to trace out the

Scheme 3. EPDimEP Pathways

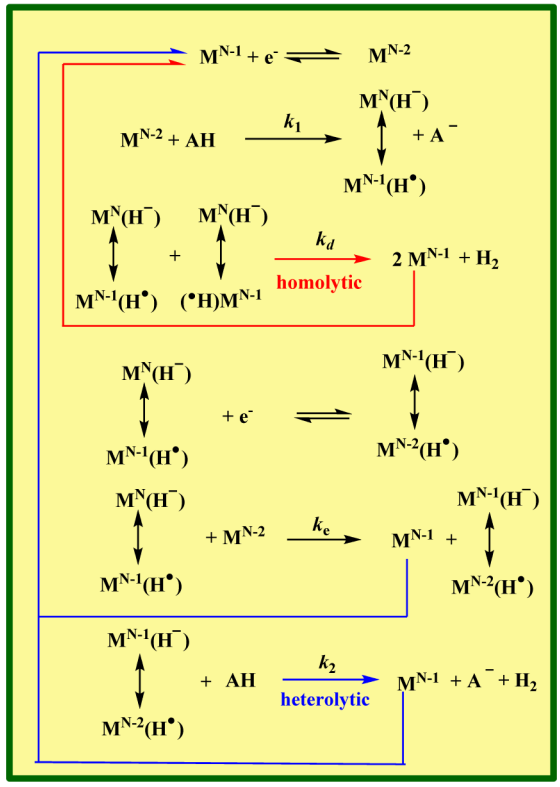

dominant reaction steps as a function of the experimental parameters is particularly helpful.

(3) The analysis was focused on fast catalytic systems under pure kinetic conditions in which side phenomena (e.g., substrate consumption, inhibition by products, and deactivation of the catalysts) have been minimized so as to give rise to canonical S-shaped CV responses independent of the scan rate (Figure 1, top right). It is noted *en passant* that for the same conditions the same analyses apply to other techniques and to preparative-scale electrolyses as well. The assumption of negligible consumption of the substrate could be lifted, with systems tending toward the conditions of total catalysis (Figure 1, top left), but this would come at the price of an increase in the number of independent parameters of the system.

(4) For the sake of simplicity, we limited ourselves to EEPDimP mechanisms (Scheme 1), but the analysis could easily be repeated for other mechanisms such as EPEDimP (Scheme 2) and EPDimPE (Scheme 3).

(5) The illustration using the reduction of Et_3NH^+, AcOH, and PhOH catalyzed by electrogenerated Fe^0TPP demonstrated the feasibility of the diagnosing strategy and may serve as a guide for future studies of other catalysts. While the first of these acids exclusively follows a heterolytic pathway, the other two provide good examples of heterolytic versus homolytic competition.

ASSOCIATED CONTENT

Supporting Information

Experimental details and derivations of the equations allowing the establishment of the kinetic zone diagram and the various expressions and working curves depicting the variations of the plateau current and half-wave potential with the appropriate

dx.doi.org/10.1021/ja505845t | J. Am. Chem. Soc. 2014, 136, 13727−13734

parameters. This material is available free of charge via the Internet at http://pubs.acs.org.

AUTHOR INFORMATION

Corresponding Authors

cyrille.costentin@univ-paris-diderot.fr
saveant@univ-paris-diderot.fr

Notes

The authors declare no competing financial interest.

REFERENCES

(1) Tard, C.; Pickett, C. J. *Chem. Rev.* **2009**, *109*, 2245.

(2) Felton, G. A. N.; Mebi, C. A.; Petro, B. J.; Vannucci, A. K.; Evans, D. H.; Glass, R. S.; Lichtenberger, D. L. *J. Organomet. Chem.* **2009**, *694*, 2681.

(3) (a) Vincent, K. A.; Parkin, A.; Armstrong, F. A. *Chem. Rev.* **2007**, *107*, 4366. (b) Armstrong, F. A.; Belsey, N. A.; Cracknell, J. A.; Goldet, G.; Parkin, A.; Reisner, E.; Vincent, K. A.; Wait, A. F. *Chem. Soc. Rev.* **2009**, *38*, 36.

(4) Gloaguen, F.; Rauchfuss, T. B. *Chem. Soc. Rev.* **2009**, *38*, 100.

(5) (a) Liebgott, P.-P.; Leroux, F.; Burlat, B.; Dementin, S.; Baffert, C.; Lautier, T.; Fourmond, V.; Ceccaldi, P.; Cavazza, C.; Meynial-Salles, I.; Soucaille, P.; Fontecilla-Camps, J. C.; Guigliarelli, B.; Bertrand, P.; Rousset, M.; Léger, C. *Nat. Chem. Biol.* **2010**, *6*, 63. (b) Abou Hamdan, A.; Liebgott, P.-P.; Fourmond, V.; Gutiérrez-Sanz, O.; De Lacey, A. L.; Infossi, P.; Rousset, M.; Dementin, S.; Léger, C. *Proc. Natl. Acad. Sci. U.S.A.* **2012**, *109*, 19916. (c) Fourmond, V.; Baffert, C.; Sybirna, K.; Lautier, T.; Abou Hamdan, A.; Dementin, S.; Soucaille, P.; Meynial-Salles, I.; Bottin, H.; Léger, C. *J. Am. Chem. Soc.* **2013**, *135*, 3926.

(6) Thoi, V. S.; Sun, Y.; Long, J. R.; Chang, C. J. *Chem. Soc. Rev.* **2013**, *42*, 2388.

(7) (a) Rakowski Dubois, M.; Dubois, D. L. *Acc. Chem. Res.* **2009**, *42*, 1974. (b) Rakowski DuBois, M.; DuBois, D. L. *Chem. Soc. Rev.* **2009**, *38*, 62.

(8) (a) Gray, H. B. *Nat. Chem.* **2009**, *1*, 7. (b) Dempsey, J. L.; Brunschwig, B. S.; Winkler, J. R.; Gray, H. B. *Acc. Chem. Res.* **2009**, *42*, 1995.

(9) Gust, D.; Moore, T. A.; Moore, A. L. *Acc. Chem. Res.* **2009**, *42*, 1890.

(10) Koper, M. T. M.; Bouwman, E. *Angew. Chem., Int. Ed.* **2010**, *49*, 3723.

(11) (a) Artero, V.; Fontecave, M. *Coord. Chem. Rev.* **2005**, *249*, 1518. (b) Tran, P. D.; Artero, V.; Fontecave, M. *Energy Environ. Sci.* **2010**, *3*, 727. (c) Artero, V.; Chavarot-Kerlidou, M.; Fontecave, M. *Angew. Chem., Int. Ed.* **2011**, *50*, 7238. (d) Artero, V.; Fontecave, M. *Chem. Soc. Rev.* **2013**, *42*, 2338.

(12) (a) Lee, C. H.; Dogutan, D. K.; Nocera, D. G. *J. Am. Chem. Soc.* **2011**, *133*, 8775. (b) Roubelakis, M. M.; Bediako, D. K.; Dogutan, D. K.; Nocera, D. G. *Energy Environ. Sci.* **2012**, *5*, 7737.

(13) (a) This catalytic reaction scheme is the exact homogeneous molecular counterpart of the reduction of Brønsted acids on platinum, with the first steps being equivalent to the Volmer step, the homolytic step of the Volmer–Tafel step, and the heterolytic step of the Volmer–Heyrovsky step.[13b] (b) Bockris, J. O.; Reddy, A. K. N. In *Modern Electrochemistry*; Plenum Press: New York, 1970; Vol. 2, Chapter 10, pp 1231–1250.

(14) Other competitive heterolytic versus homolytic mechanisms with different sequencing of the electron transfer, proton transfer, and dimerization steps are possible. They will be envisaged later on.

(15) (a) Collman, J. P.; Wagenknecht, P. S.; Lewis, N. S. *J. Am. Chem. Soc.* **1992**, *114*, 5665. (b) Collman, J. P.; Ha, Y.; Wagenknecht, P. S.; Lopez, M. A.; Guilard, R. *J. Am. Chem. Soc.* **1993**, *115*, 9080.

(16) (a) Dempsey, J. L.; Winkler, J. R.; Gray, H. B. *J. Am. Chem. Soc.* **2010**, *132*, 1060. (b) Dempsey, J. L.; Winkler, J. R.; Gray, H. B. *J. Am. Chem. Soc.* **2010**, *132*, 16774. (c) Valdez, C. N.; Dempsey, J. L.; Brunschwig, B. S.; Winkler, J. R.; Gray, H. B. *Proc. Natl. Acad. Sci. U.S.A.* **2012**, *109*, 15589.

(17) (a) Solis, B. H.; Hammes-Schiffer, S. *Inorg. Chem.* **2011**, *50*, 11252. (b) Solis, B. H.; Hammes-Schiffer, S. *J. Am. Chem. Soc.* **2011**, *133*, 19036.

(18) Muckerman, J. T.; Fujita, E. *Chem. Commun.* **2011**, *47*, 12456.

(19) Hu, X.; Brunschwig, B. S.; Peters, J. C. *J. Am. Chem. Soc.* **2007**, *129*, 8988.

(20) (a) Razavet, M.; Artero, V.; Fontecave, M. *Inorg. Chem.* **2005**, *44*, 4786. (b) Baffert, C.; Artero, V.; Fontecave, M. *Inorg. Chem.* **2007**, *46*, 1817. (c) Bhattacharjee, A.; Andreiadis, E. S.; Chavarot-Kerlidou, M.; Fontecave, M.; Field, M. J.; Artero, V. *Chem.—Eur. J.* **2013**, *19*, 15166.

(21) Savéant, J.-M. *Elements of Molecular and Biomolecular Electrochemistry: An Electrochemical Approach to Electron Transfer Chemistry*; John Wiley & Sons: Hoboken, NJ, 2006; pp 121–125.

(22) (a) Costentin, C.; Savéant, J.-M. *ChemElectroChem* **2014**, *1*, 1226. (b) Savéant, J.-M.; Su, K.-B. *J. Electroanal. Chem.* **1984**, *171*, 341. (c) See p 109 in ref 21.

(23) Bhugun, I.; Lexa, D.; Savéant, J.-M. *J. Am. Chem. Soc.* **1996**, *118*, 3982.

(24) Izutsu, K. *Electrochemistry in Nonaqueous Solvents*; Wiley-VCH: Weinheim, Germany, 2002; Chapter 3.

(25) (a) Besides substrate consumption, the main side phenomena are inhibition by products and deactivation of the catalyst. These effects increase with the charge passed during the CV experiment and are therefore minimized by raising the scan rate.[25b] (b) Costentin, C.; Drouet, S.; Robert, M.; Savéant, J.-M. *J. Am. Chem. Soc.* **2012**, *134*, 11235.

(26) These values are in good agreement with those previously determined under total catalysis conditions.[23]

(27) These simulations were performed using the DigiElch software. See: Rudolph, M. *J. Electroanal. Chem.* **2003**, *543*, 23.